THE JOURNAL OF BIOLOGICAL CHEMISTRY VOL. 285, NO. 4, pp. 2721–2733, January 22, 2010

Structural Insights into the Specificity of Xyn10B from *Paenibacillus barcinonensis* and Its Improved Stability by Forced Protein Evolution*

Received for publication, September 16, 2009, and in revised form, October 28, 2009 Published, JBC Papers in Press, November 23, 2009, DOI 10.1074/jbc.M109.064394

Óscar Gallardo[‡], F. I. Javier Pastor[‡1], Julio Polaina[§], Pilar Diaz[‡], Robert Łysek[¶], Pierre Vogel[¶], Pablo Isorna[‖], Beatriz González[‖], and Julia Sanz-Aparicio[‖]

From the [‡]Department of Microbiology, Faculty of Biology, University of Barcelona, Av. Diagonal 645, 08028 Barcelona, Spain, the [§]Instituto de Agroquímica y Tecnología de Alimentos, Consejo Superior de Investigaciones Científicas, Apdo. 73, 46100-Burjassot, Valencia, Spain, the [¶]Laboratoire de Glycochimie et de Synthèse Asymétrique, Ecole Polytecnique Fédérales de Lausanne, Institute of Chemical Sciences and Engineering, Biological Chemistry, CH-1015 Lausanne-Dorigny, Switzerland, and the [‖]Instituto de Química-Física "Rocasolano," Consejo Superior de Investigaciones Científicas, Serrano 119, 28006 Madrid, Spain

Paenibacillus barcinonensis **is a soil bacterium bearing a complex set of enzymes for xylan degradation, including several secreted enzymes and Xyn10B, one of the few intracellular xylanases reported to date. The crystal structure of Xyn10B has been determined by x-ray analysis. The enzyme folds into the typical $(\beta/\alpha)_8$ barrel of family 10 glycosyl hydrolases (GH10), with additional secondary structure elements within the β/α motifs. One of these loops -L7- located at the β7 C terminus, was essential for xylanase activity as its partial deletion yielded an inactive enzyme. The loop contains residues His^{249}–Glu^{250}, which shape a pocket opened to solvent in close proximity to the +2 subsite, which has not been described in other GH10 enzymes. This wide cavity at the +2 subsite, where methyl-2,4-pentanediol from the crystallization medium was found, is a noteworthy feature of Xyn10B, as compared with the narrow crevice described for other GH10 xylanases. Docking analysis showed that this open cavity can accommodate glucuronic acid decorations of xylo-oligosaccharides. Co-crystallization experiments with conduramine derivative inhibitors supported the importance of this open cavity at the +2 subsite for Xyn10B activity. Several mutant derivatives of Xyn10B with improved thermal stability were obtained by forced evolution. Among them, mutant xylanases S15L and M93V showed increased half-life, whereas the double mutant S15L/M93V exhibited a further increase in stability, showing a 20-fold higher heat resistance than the wild type xylanase. All the mutations obtained were located on the surface of Xyn10B. Replacement of a Ser by a Leu residue in mutant xylanase S15L can increase hydrophobic packing efficiency and fill a superficial indentation of the protein, giving rise to a more compact structure of the enzyme.**

Biodegradation of xylan, an abundant plant polysaccharide, is a complex process that requires the coordinate action of several enzymes, among which xylanases (1,4-β-D-xylan xylanohydrolase; EC 3.2.1.8), cleaving internal linkages on the β-1,4-xylose backbone, play a key role. The complex chemical nature and heterogeneity of xylan can account for the multiplicity of xylanases produced by microorganisms (1, 2). The activity of different xylanases with subtle differences in substrate specificity and mode of action contributes to improving the degradation of plant xylan in natural habitats. Based on amino acid sequence homologies and hydrophobic cluster analysis, xylanases have been classified in two main groups in glycoside hydrolase families 10 and 11 (CAZy, 3), although a few characterized xylanases have recently been ascribed to glycoside hydrolase families 5, 7, 8, and 43 (2, 4, 5). GH10 xylanases fold into a $(\beta/\alpha)_8$ barrel (6, 7), whereas GH11 enzymes display a β-jelly roll structure (8, 9). Besides the remarkable differences in sequence, structure, and reaction mechanism (10), xylanases show subtle differences in substrate specificity (11, 12). Among these differences, GH10 enzymes are capable of cleaving glycosidic linkages in the xylan main chain closer to the substituents than GH11 xylanases do, thus yielding smaller hydrolysis products from glucuronoxylan (13). Analysis of the crystal structure of *Cellvibrio mixtus* Xyn10B (14), *Streptomyces olivaceoviridis* Xyn10A (15), and *Thermoascus aurantiacus* Xyn10 (16) in complex with side chain-substituted xylo-oligosaccharides has shown that the substrate-binding site of GH10 enzymes is able to accommodate decorated regions of xylan, and in fact a role for the xylan side chains as determinants of specificity for GH10 xylanases has been proposed (16).

Biotechnological applications of xylanases are of increasing importance because of their enormous potential to modify and transform lignocellulosic biomass, used in a wide variety of industrial processes, and for the bioconversion of agricultural wastes into fermentable sugars (17–19). Stability in the conditions of industrial processes is a usual requisite for an enzyme to be successfully applied in biotechnology. Comparison of structures of thermophilic enzymes with their mesophilic homologues and directed evolution studies show that high stability can be achieved by many strategies (20), and in many examples

* This work was supported in part by Spanish Ministry of Education and Science Grant BIO2007-67708-C04-04.

The atomic coordinates and structure factors (codes 3EMC, 3EMQ, and 3EMZ) have been deposited in the Protein Data Bank, Research Collaboratory for Structural Bioinformatics, Rutgers University, New Brunswick, NJ (http://www.rcsb.org/).

[1] To whom correspondence should be addressed. Tel.: 34-93-4034626; Fax: 34-93-4034629; E-mail: fpastor@ub.edu.

a very limited number of point mutations can lead to large stability differences (21). The residues on the surface of the proteins can notably contribute to enzyme folding and resistance to denaturation (20, 22). Besides the contribution of charged surface residues and salt bridges to protein stability, it has been shown that incorporation of hydrophobic residues at the protein surface can increase packing in a surface indentation or cavity, with a subsequent stabilization effect (23). Variation of surface residues may provide a powerful approach to increase the thermal stability of an enzyme (24).

Xylanases are secreted enzymes, released to the extracellular medium to enable contact with and cleavage of highly polymerized xylans. However, a few examples of GH10 xylanases have been proposed to have an intracellular location, where they are probably involved in the hydrolysis of small xylo-oligomers resulting from the activity of extracellular enzymes. One of these intracellular xylanases, *C. mixtus* Xyn10B is a periplasmic enzyme (25), whereas *Paenibacillus barcinonensis* Xyn10B and *Aeromonas caviae* XynX have been clearly shown to be located in the cytoplasm (26, 27). *P. barcinonensis* is a powerful xylanolytic soil bacteria recently taxonomically identified (28), which in addition to intracellular Xyn10B produces a set of secreted xylanases, some of which have been successfully evaluated in paper biotechnology (29–31). *P. barcinonensis* Xyn10B is highly homologous to six xylanases of the GH10 family (XynX from *A. caviae* (32), XynA2 from *Bacillus stearothermophilus* T-6 (33), XyaA from *Bacillus* sp. N137 (34), Xyn2 from *B. stearothermophilus* 21 (35), XynA from *Thermobacillus xylanilyticus* (36), and XynA from *Caldicellulosiruptor saccharolyticus* (37)) that similar to Xyn10B do not exhibit a signal peptide sequence. These signal peptide-less xylanases form a distinctive group of enzymes that cluster separately from the rest of GH10 xylanases and seem to constitute a new type of xylanases (26). *P. barcinonensis* Xyn10B shows high activity on small substrates, as aryl-xylosides and xylo-oligosaccharides (26, 38), in agreement with its cytoplasmic location, where it should cleave oligomers resulting from extracellular xylan hydrolysis. In this study, we have analyzed the crystal structure of Xyn10B and found distinctive features in its catalytic site that can facilitate binding to decorated xylo-oligosaccharides. A series of mutant derivatives with an increased thermal stability have been obtained by forced evolution, evidencing the importance of surface interactions in Xyn10B folding. The results we have found contribute to deciphering the biochemical function of intracellular xylanases. The few existing reports on the catalytic properties of intracellular xylanases make it difficult to identify common traits that can give clues to understanding their contribution to xylan hydrolysis. Further studies will be required to ascertain their role in degradation of xylan in natural habitats.

EXPERIMENTAL PROCEDURES

Bacterial Strains and Plasmids—Plasmid pX60, containing the *xyn10B* gene from *P. barcinonensis* cloned in pUC19, has been described previously (38). It was used as a template for PCR amplification and gene shuffling. Plasmid pET3b (Novagen) was used as a plasmid vector to express wild type *xyn10B*. *Escherichia coli* BL21(DE3) (Novagen) was used as a host strain for pET3b-*xyn10B* to obtain high protein expression of Xyn10B for purification and crystallization. *E. coli* DH5α was used as host strain for cloning and expression of the *xyn10B* mutants. In those mutants, pGEM®-T-easy plasmid (3015 bp, from Promega) was used as cloning vector for A-protuberant *Taq* polymerase amplicons.

Random Mutagenesis and Screening for Thermoresistant Xylanase Mutants—Random mutagenesis of *xyn10B* was carried out by error-prone PCR amplification (39, 40), where one of the four nucleotides was in excess, or by standard PCR amplification, followed by DNA shuffling. In all cases *Taq*DNA polymerase (without proofreading activity) was used.

The oligonucleotides used as primers for the amplification of the *xyn10B* open reading frame from pX60 plasmid were CL1 5′-AGCGGATAACAATTTCACACAGGA-3′ in the direct orientation and CL3 5′-CGCCAGGGTTTTCCCAGTCACGAC-3′ in the reverse orientation. Error-prone PCR amplification was performed basically as described by Gonzalez-Blasco *et al.* (41).

DNA shuffling reactions were carried out as described by Stemmer (42) with some modifications. Amplified *xyn10B* gene, either by standard or error-prone PCR, was treated with DNase. DNA fragments between 50 and 150 bp were purified with a QIAquick gel extraction kit (Qiagen) and reassembled in a PCR without primers (PCR I) in a 50-μl volume for 20–45 cycles of amplification. The reassembly product was 1:40 or 1:100 diluted and used as template in an additional PCR run with primers CL1 and CL3 (PCR II) in a final volume of either 25 or 100 μl for 10–15 cycles of amplification. Samples from DNA shuffling reactions were ligated into the pGEM®-T-easy plasmid and transformed into *E. coli* DH5α, selecting for ampicillin resistance and white color colonies.

Clones with thermoresistant Xyn10B activity were identified by the plate assay described by López-Camacho and Polaina (43). Plates containing transformant clones were incubated at temperatures that cause inactivation of wild type Xyn10B, 60–80 °C 30 min, and then assayed for residual activity by overlaying with the chromogenic substrate *p*NPX.[2]

Site-directed Mutagenesis and DNA Sequencing—Site-directed mutagenesis was performed by PCR amplification with primers designed to include the mutated nucleotides (BKE137D, 5′-ccgtcttgtc**A**tcaatcgcc-3′; BKD323N, 5′-gaat-**T**cttgggctgaagctctg-3′; BKS15L, 5′-gaac**A**aattggcataagatgcag-3′; and BKM93V, 5′-caaaca**C**ccaagccggcgtc-3′) and the corresponding forward primers containing the wild type nucleotide sequences (FWE137D, 5′-ATCTGATTATGCGTGATACAAAATG-3′; FWD323N, 5′-CTTCTGGCGTATTATCGGGC-3′; FWS15L, 5′-AAAATAGGTGCGGCAGTGC-3′; and FWM93V 5′-AAGATGCTTCCGGGGGAACG-3′) following the procedure described by Mikaelian and Sergeant (44). Wild type and mutant versions of the *xyn10B* gene were sequenced by the Sanger procedure using internal and external primers.

Xylanase Purification—Wild type Xyn10B and mutant xylanases were purified from *E. coli* recombinant cultures. Cells

[2] The abbreviations used are: *p*NPX, *p*-nitrophenol-β-D-xylopyranoside; MPD, methyl-2,4-pentanediol; PEG, polyethylene glycol.

were collected and disrupted by French press; cell extracts were treated with streptomycin sulfate to eliminate nucleic acids by ultracentrifugation, and proteins were concentrated by ammonium sulfate precipitation. Concentrated extracts were subjected to gel filtration (HiLoad™ 16/60 Superdex™ 75 prep grade column, GE Healthcare) followed by anion exchange chromatography (Tricorn™ Mono Q™ 5/50 GL, GE Healthcare) on a fast protein liquid chromatography system (ÄKTA™ FPLC™, GE Healthcare). On some occasions, a polishing step in a second gel filtration column was performed (Tricorn™ Superdex™ 200 10/300 GL, GE Healthcare).

Activity Assays—Xylanase activity was assayed by determining the amount of *p*-nitrophenol released from *p*NPX (Sigma). The assay mixture contained 5 mM *p*NPX (for usual assays) or 0.1–10 mM *p*NPX (for kinetic assays) in a final volume of 0.2 ml of 50 mM acetate buffer, pH 5.5. The assay mixture was incubated at 35 °C for 15 min, and color development was measured at 400 nm. One unit of enzymatic activity was defined as the amount of enzyme that releases 1 μmol of *p*-nitrophenol/min under the assay conditions described.

Irreversible thermal inactivation of purified xylanases was determined as described by López-Camacho *et al.* (45). Thermal inactivation was modeled as a first-order kinetic process, and the half-life (t_m) of the enzymes was determined from the first-order rate constants of inactivation, corresponding to the slopes of the lines obtained by plotting ln (percentage of residual activity) *versus* incubation time. Kinetic parameters (V_{max}, K_m, and k_{cat}) were determined by fitting hyperbolic Michaelis-Menten curves with the program SigmaPlot version 4.00 (Jandel Scientific).

Thin Layer Chromatography—TLC was performed as described previously (38). Silica gel plates 60F254 were used (Merck). The solvent used was chloroform/acetic acid/water (3:6:1, v/v). Oligosaccharides were detected by spraying the plates with an ethanol/concentrated sulfuric acid mixture (95:5, v/v) and heating at 121 °C for 5–10 min.

Crystallization and Data Collection—Equal amounts of protein solution (10 mg/ml Xyn10B in 10 mM Tris-HCl, pH 7) and precipitant buffer (35% (v/v) MPD, 17% (w/v) PEG 3350 in 100 mM Tris, pH 7) were mixed and vapor-equilibrated against a reservoir containing the latter solution. Crystallization experiments were carried out at room temperature. Long needles grew in 2–3 days to maximum size 0.02, 0.02, 1.0 mm^3. They belong to $P2_12_12_1$ space group, with 1 molecule per asymmetric unit and 40% solvent content in the cell. For data collection, native crystals were transferred to cryoprotectant solutions containing 40% (v/v) MPD, 20% (w/v) PEG 3350 before being cooled to 120 K in a stream of nitrogen (Oxford Instruments). An x-ray radiation (CuK_α) data set was collected using an in-house Bruker-Nonius rotating anode generator, operating at 40 kV and 100 mA, equipped with Osmic focusing mirrors and Kappa2000 CCD detector. A total of 245 data frames were collected using 0.5° oscillations and 5-min exposure times. The diffraction data were analyzed with HKL-2000 (46) package to yield integrated intensities. A summary of data collection and data reduction statistics is shown in Table 1.

Structure Solution and Refinement—The structure of Xyn10B was solved by the molecular replacement method. Initial phases were obtained with the MOLREP program (47) using the atomic coordinates of xylanase XT6 from *Geobacillus stearothermophilus* as the search model (Protein Data Bank code 1HIZ). A clear solution was found, which after rigid-body fitting produced an *R*-factor of 0.51 with a correlation coefficient of 0.37 for data up to 3 Å. Crystallographic refinement was performed by using CNS (48) with flat bulk-solvent correction, including low resolution data to 50 Å, and using maximum likelihood target features. A subset of 7% randomly selected structure-factor amplitudes was excluded from automated refinement to compute a free *R*-factor throughout the refinement. Several rounds of simulated annealing refinement were alternated with rebuilding by the program O (49). At the last stage, water molecules were included and were combined with more rounds of positional and individual restrained *B*-factor refinement, which led to a final *R*-factor of 0.19 (R_{free} = 0.25) for all data set up to 2.1 Å resolution. Final refinement parameters are reported in Table 1. Stereochemistry of the model was checked by using PROCHECK (50) and MOLPROBITY (51), and the figures were generated with PyMOL (52).

To get the complexes, crystals were transferred into a fresh solution containing 10 mM inhibitor and 40% (v/v) PEG 4000 (in the case of R115) or PEG 400 (in the case of R117), and 20% (w/v) PEG 3350 in 100 mM Tris, pH 7. After soaking overnight, the crystals were flash-frozen to 120 K. Simulated annealing omit maps were calculated at the active-site cavity showing the presence of the inhibitors at the active center. They were manually built into the model and included in the refinement. Final statistics are given in Table 1.

Automated Docking of Decorated Xylotriose into Xyn10B Structure—Xylotriose chain ligands decorated in the internal ring with 4-*O*-Me-glucuronic acid (at O2) or arabinose (at O3) were manually built from the ligand-bound protein complexes of CmXyn10B retrieved from Protein Data Bank entries 1UQZ and 1UR1. All hydrogen atoms were added to the ligands, and charges were assigned by the Gasteiger method using the AutoDockTools program (53). All glycoside linkages were defined as rotatable bonds. The protein model contains the coordinates of the Xyn10B crystal structure presented here but blocking the glycone (minus) part of the active-site channel with a fixed xylotriose chain in a position inferred from structural superposition of Xyn10B to CmXyn10B. In this way, we investigated the binding of the ligands at the aglycone (plus) portion of the active site.

Autodock 4.0 was executed 50 times with the Lamarckian genetic algorithm (54), a population size of 150, elitism set at 1, mutation rate at 0.02, and crossover rate of 0.80. Simulations were performed with a maximum of 2,500,000 energy evaluations and a maximum of 27,000 generations. Docking results were clustered using a cut-off of 2 Å root mean square deviations.

RESULTS

Crystal Structure of Xyn10B Shows the Active-site Architecture—The crystal structure of native Xyn10B was solved at 2.1-Å resolution. Experimental details and structure determination procedures are given under "Experimental Procedures" and in Table 1. Crystals belong to the $P2_12_12_1$ space

TABLE 1
X-ray data collection and structure refinement statistics

	Crystal		
	1 Xyn10B	2 Xyn10B-R115	3 Xyn10B-R117
A. Data collection			
Unit cell dimensions	43.93, 79.11, 91.43 Å	44.39, 79.64, 92.41 Å	44.02, 79.72, 91.18 Å
Limiting resolution	2.1 Å	2.7 Å	2.0 Å
(outer shell)	(2.15 to 2.07)	(2.87 to 2.73)	(2.14 to 2.05)
Unique reflections	20,958	9262	20,971
R_{sym} [a]	0.10 (0.43)	0.14 (0.59)	0.12 (0.52)
Completeness	99.0% (96.1%)	99.0% (99.4%)	99.6% (99.5%)
Mean multiplicity	6.5 (3.2)	6.0 (3.9)	4.3 (3.1)
Mean $I/\sigma I$	10.0 (2.1)	10.1 (3.1)	8.9 (2.5)
B. Final refinement parameters			
Protein atoms (non-H)	2714	2714	2714
Ligand atoms (non-H)	16	26	32
Solvent molecules	279	265	279
R-factor [b]	0.19	0.21	0.22
R_{free}	0.25	0.29	0.26
Root mean square bonds/angles	0.007 Å/1.3°	0.007 Å/1.3°	0.007 Å/1.3°
Averaged *B*-factors			
Main chain	13.3 Å^2	25.1 Å^2	34.6 Å^2
Side chain	15.3 Å^2	26.1 Å^2	35.6 Å^2
Ligand	28.3 Å^2	34.4 Å^2	56.2 Å^2
Ramachandran plot (MOLPROBITY)			
Favored	99.5%	98.9%	99.5%
Allowed (%)	0.5%	1.1%	0.5%
PDB codes	3EMC	3EMQ	3EMZ

[a] $R_{sym} = \Sigma|I(h)I - \langle I(h)\rangle/\Sigma\langle I(h)\rangle$.
[b] *R*-factor $= \Sigma(||F_{obs} - F_{calc}|)/\Sigma|F_{obs}|$ (R_{free} is equivalent to *R*-factor for a randomly selected 7% subset of reflections not used in structure refinement).

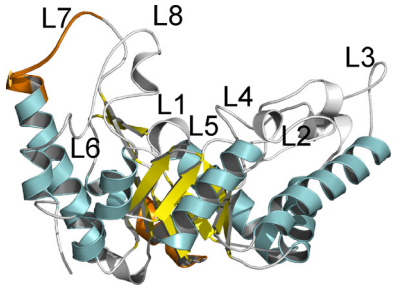

FIGURE 1. **Overall structure and active-site architecture of Xyn10B.** The typical $(\beta/\alpha)_8$ barrel fold of GH10 xylanases is represented in *cyan* (helices) and *yellow* (strands). The long loops (*gray*) at the C terminus of the β-strands define a salad bowl shape defining an extended groove consistent with its *endo* mode of action and suitable to allocate polymeric substrates. The motifs a (AIE_YASL) and b (RTDL__PT_EM), characteristic of signal peptide-less xylanases, are highlighted in *orange*. Region a is located in helix α6, whereas region b is located in loop L7, which is directly involved in substrate recognition and binding.

group, with one molecule in the asymmetric unit and 40% solvent content within the cell. The structure of the monomeric Xyn10B corresponds to the topology of a single $(\beta/\alpha)_8$ barrel, as expected for family 10 glycosidases (CAZy). The barrel is closely packed in the face corresponding to the short loops linking different β/α repeats, whereas additional secondary structure elements are included within the β/α motifs (Fig. 1). These long segments at the C terminus of the β-strands (L1 to L8) are defining the active center, the catalytic residues being located at the end of β4 (the acid/base Glu^{134}) and β7 (the nucleophilic Glu^{241}), respectively. This specific setting of the catalytic residues is a conserved feature along other retaining β-glycosidases that altogether define the clan GH-A superfamily (CAZy). In the particular case of GH10, the long L1–L8 loops give a "salad bowl" shape to the macromolecule, defining an extended open cleft consistent with its endo-mode of attack and able to accommodate polymeric substrates. Fig. 2*A* displays the molecular surface of Xyn10B showing an open and extended active-site groove, in which two 2-methyl-2,4-pentanediol molecules (MPD1 and MPD2) from the crystallization medium have been found.

Xyn10B belongs to a group of signal peptide-less xylanases showing the conserved amino acid sequences AIE_YASL (region a) and RTDL__PT_EM (region b) as distinctive features not found in other GH10 xylanases (26). The first of these regions is located in helix α6, whereas region b is located in loop L7 and also includes the two amino acids at the N terminus of helix α7 (Fig. 1). Region b is located between the conserved regions VI and VII of GH10 xylanases (55), making the spacing between these conserved regions in signal peptide-less xylanases longer than in many extracellular xylanases. To evaluate the importance of region b (residues 253–263) on the catalytic activity of Xyn10B, and before the crystal structure became available, a series of amino acid deletions were introduced in the enzyme by directed mutagenesis. Three xylanase mutants were constructed that showed increasing deletions in this region. The mutant with the shortest deletion (Δ253–256) was only deleted in the four amino acids -RTDL- of the N terminus of region b, whereas mutants Δ253–260 and Δ249–261 were deleted in an increasing portion covering the complete region b except for the two EM residues of its C terminus. Neither of the mutants constructed showed enzyme activity, which indicated that this nonstructured region, in close proximity to the binding cleft of the enzyme, was essential for the catalytic activity of Xyn10B. As shown in Fig. 1, L7 together with L4 and L8 are the long loops shaping the extended active-site cleft, and in particular, His^{249}–Glu^{250}, at the beginning of L7, are directly involved in substrate recognition, as shown below.

Two structures from intracellular xylanases have been reported to date as follows: that from *G. stearothermophilus* (GsXynB, see Ref. 56) and that from *C. mixtus* (CmXyn10B), the latter being solved in complex with a xylo-oligosaccharide

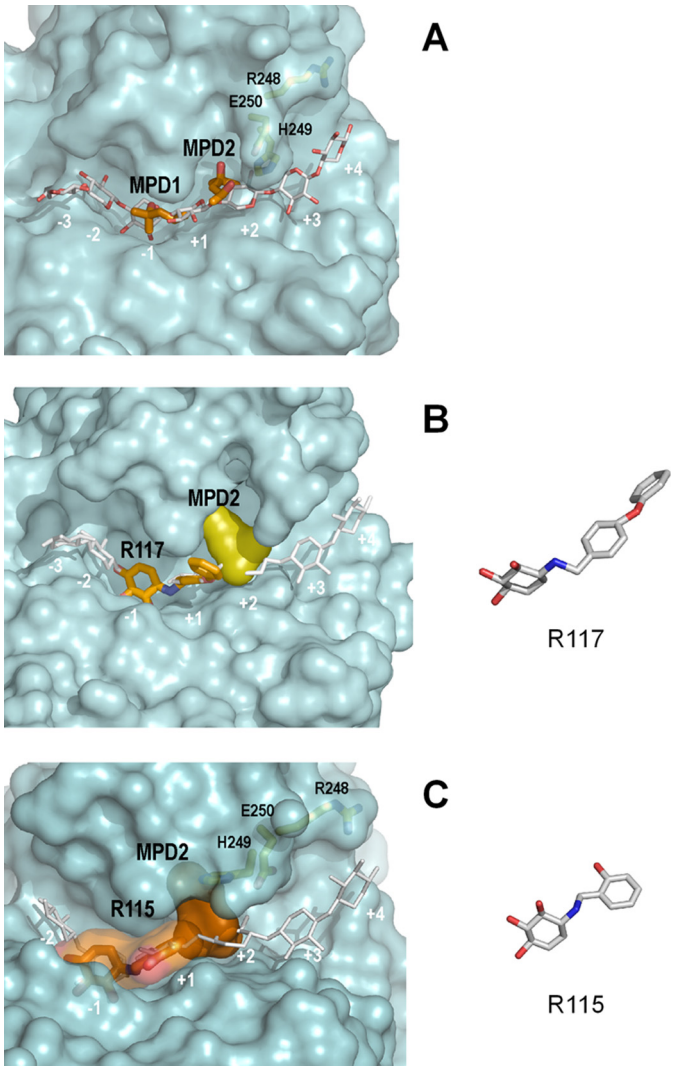

FIGURE 2. **Active-site cleft of Xyn10B.** Molecular surface of the enzyme showing the occupation of the different structures solved: as follows: native crystals contain two molecules of MPD colored in *orange* (*A*), whereas only MPD1 has been substituted in the two complexes by the corresponding inhibitors R117 (*B*) or R115 (*C*). A xylo-oligosaccharide chain has been docked into the cleft by structural superposition of Xyn10B coordinates to the complex of CmXynB10 (Protein Data Bank code 1UQY), allowing the active-site mapping. As *B* illustrates, the steric hindrance of MPD2 precludes full entrance of the three-rings inhibitor R117 into the cleft. The L7 segment Arg^{248}–His^{249}–Glu^{250} is represented as *sticks* showing the conformational change upon R115 inhibitor binding.

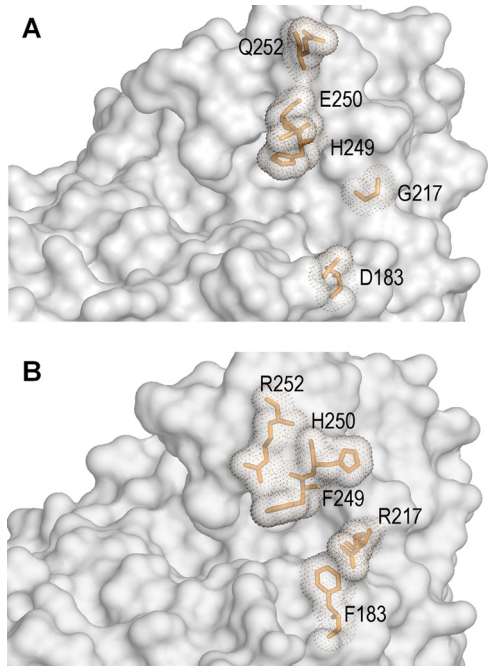

FIGURE 3. **Comparison of Xyn10B with GsXynB.** Active site cleft of Xyn10B (*A*) in the same view as GsXynB (*B*) showing the different conformation of the segment 249–252 found in both enzymes, which shapes a narrow and shorter pocket in GsXynB, delimited by Phe^{183} and Arg^{217}. Conversely, the active-site cleft of Xyn10B seems able to accommodate long and branched substrates.

chain (14). Therefore, in an attempt to have a subsite mapping of the binding cleft, the coordinates of Xyn10B were superimposed to those of CmXyn10B complexed with xylopentaose (Protein Data Bank code 1UQY). In this complex, a xylotriose and a xylotetraose were observed at the glycone (minus) and aglycone (plus) subsites, respectively, following the nomenclature used for sugar-binding subsites, which defines that the cleavage occurs between subsite −1, +1 (57, 58).

The structural overlap of both enzymes reveals an inferred position for the oligosaccharide chain, shown in Fig. 2*A*, that fits well into the Xyn10B groove, suggesting that this enzyme can accommodate an elongated sugar chain and may display specific binding to at least four xylose units, *i.e.* those positioned from −2 to +2 subsites. Moreover, one of the MPD molecules mentioned, MPD1, is located in a position that could mimic the putative scissile glycosidic bond (−1, +1), whereas the other, MPD2, is placed deeper in a pocket connected to subsite +2. In fact, the wide cavity observed at subsite +2 is a noteworthy feature of Xyn10B, as compared with the narrow crevice described for other GH10 enzymes. In particular, the highly homologous enzyme GsXynB has been described to have a rather small and narrow cleft able to allocate only short and unbranched oligoxylose substrates (56). A comparison between these two enzymes (Fig. 3) shows that Phe^{183} and Arg^{217} side chains are blocking the aglycone active site of GsXynB at the plus subsites, whereas the corresponding residues in Xyn10B, Asp^{183} (L5) and Gly^{217} (L6), leave an open, extended cleft allowing the accommodation of possible xylose rings at subsites +3 and +4. In addition, the different conformation adopted by the segment Phe^{249}–Arg^{252} in GsXynB shapes a narrow pocket in which the bulky side chain of Arg^{252} precludes the wide cavity observed in Xyn10B.

Furthermore, reported studies on complexed CmXyn10B (14) and other GH10 xylanases (15, 16) in complex with decorated xylo-oligosaccharides have shown that xylan substitutions can be accommodated only in selected subsites in which the O2 and O3 of xylose point into the solvent, *i.e.* −3, −2, +1, and +3, although in the case of the −1 and +2 subsites, the hydroxyls are directed into the protein surface therefore occluding binding of side-chain xylan decorations. As it can be observed in Fig. 2*A*, the active site of Xyn10B seems able to allocate also a branched xylose unit at subsite +2, as the putative O2 and O3 are pointing to a pocket also open to the solvent. In fact, the MPD2 molecule found in the crystal of uncomplexed Xyn10B seems to emulate a possible substitution at the

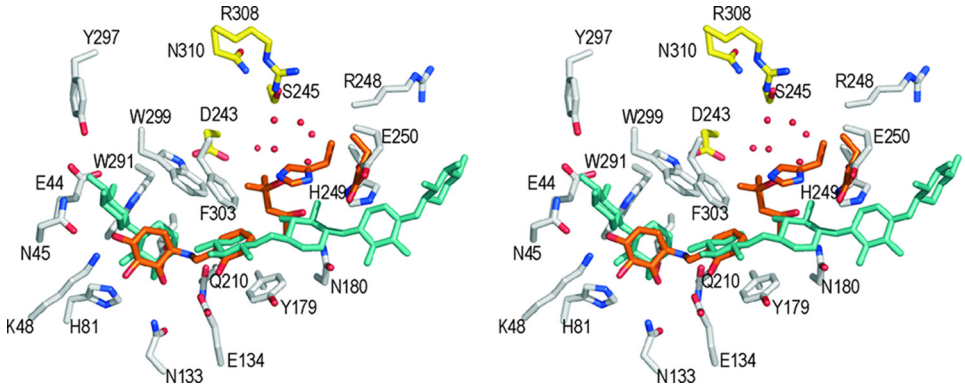

FIGURE 4. **Recognition mode of the inhibitor by Xyn10B.** Stereo view of the active site of the native enzyme (*white*) and the Xyn10B-R115 complex (*orange*) showing the atomic interactions in detail and the change in the position of His^{249} and Glu^{250} (*orange*) found in the complex. The conduramine ring at subsite −1 is linked by polar interactions to Xyn10B as follows: N1, to Glu^{134} and Gln^{210}; O2, to Asn^{133}; O3, to Lys^{48} and His^{81}; O4, to Asn^{45} and Trp^{291}. At +1 subsite, the aromatic ring of the inhibitor is stacking between Trp^{299} and Phe^{303} on one side and Tyr^{179}, which is tilted in the complex, on the other side. MPD2 (*orange*) is positioned in a polar cavity filled with well ordered water molecules that make a network of hydrogen bonds to Asp^{243}/Ser^{245} from strand $\beta 7$, and Arg^{308}/Asn^{310} from loop L8, colored in *yellow*. The xylo-oligosaccharide chain (*cyan*), docked as explained in Fig. 2, confirms the identification of subsite −1, +1, and +2. As it can be seen, MPD2 mimics a putative decoration of xylose at subsite +2.

xylose postulated in this position. On the other hand, the shape of this pocket is modulated by Arg^{248}, His^{249}, and Glu^{250}, belonging to the L7 loop, which, as stated before, contains the conserved region b of signal peptide-less xylanases.

Inhibition of Xyn10B by Conduramine Derivatives Illustrates the Major Features of the Active Site—*N*-Benzyl derivatives of conduramine B-1 are good competitive inhibitors of glucosidases (59). We evaluated the activity of two new derivatives of conduramine B-1, R115 ((1*S*,2*S*,3*R*,6*R*)-6-(2-hydroxybenzylamino)cyclohex-4-ene-1,2,3-triol) and R117 ((1*S*,2*S*,3*R*,6*R*)-6-(4-phenoxybenzylamino)cyclohex-4-ene-1,2,3-triol), as inhibitors of Xyn10B. They differ widely in the size of the side group *N*-linked to conduramine. Although R115 has two units (conduramine and an aromatic ring), R117 has three units (conduramine and two aromatic rings). Inhibition assays performed with these derivatives showed that R117 caused strong inhibition, as only 3% of the initial activity was detected, whereas in the presence of R115 activity was only reduced to 56%. The higher inhibition caused by the three units of inhibitor *versus* the inhibitor of two units points to the importance of the +2 subsite for catalytic activity.

To further investigate how the inhibitors bind into the active site of Xyn10B, co-crystallization experiments with R115 and R117 were carried out. As this approach failed, soaking experiments of Xyn10B crystals into inhibitor-containing crystallization mother liquid were performed. However, after diffraction data processing, the calculated electron density maps of both crystals showed that the inhibitors were not able to fully displace the two MPD molecules tightly bound at the active site of native Xyn10B crystals. In the case of R115, the inhibitor was not observed at all in the maps, and the two MPD molecules were still visible and well ordered in density (data not shown). In the R117 soaked crystals, the density showed a molecule of inhibitor at the active-site cleft substituting MPD1 but not MPD2, which was not displaced thus preventing proper occupation of the active site by the inhibitor molecule (Fig. 2*B*). In an attempt to get the correct Xyn10B-inhibitor complexes, the high content of MPD (30% MPD, 17% PEG 3350) was removed from the crystal soaking solution. Thus, R117 was dissolved in a solution in which the MPD was substituted by PEG 400, a polymer that is commonly used in crystallization experiments as an alternative to MPD. This soaking yielded similar results to those found previously (Fig. 2*B*), indicating that even in absence of saturating MPD conditions, MPD2 keeps tightly bound to Xyn10B. In the case of R115, the inhibitor was solved in a soaking solution where MPD had been substituted by PEG 4000, a change in the soaking conditions that finally allowed full entrance of the inhibitor into the active site of Xyn10B, as shown in Fig. 2*C*.

As Fig. 2*B* shows, and according to its role as a transition-state analogue, R117 binds at the same position as the modeled −1, +1 xylose, hence validating the previously suggested subsite mapping. However, the steric hindrance produced by the bound MPD2 prevents full entrance of the inhibitor into the active-site cleft, its phenyl moiety being pushed away and displaced out of the active site in an orientation not well defined in the electron density maps, which is expected from the fact that it does not make any interaction with the active-site residues that fix its position. Fig. 2*C* shows that R115 is located also in the −1, +1 subsites, and the most significant difference between both complexes is a change in the conformation of His^{249} and Glu^{250} side chains, which results in a narrower active-site cleft and a closer position of the His^{249} to subsite +2 than in the Xyn10B-R117 complex and in the native enzyme.

Recognition Mode Is Suggested by the Atomic Interactions within the Active Site of Xyn10B—Fig. 4 displays a close view of the active site of Xyn10B showing the recognition details of inhibitor R115 by the enzyme. Interaction of the conduramine ring at the −1 subsite is very similar to that of a bound xylose as described for other GH10 xylanases, with the sugar ring being perpendicular to the conserved Trp^{299}. The N1, which is mimicking the glycosidic *O*-link, is hydrogen bonded to the catalytic Glu^{134} and also to Gln^{210}. The O2 is linked to Asn^{133}, whereas O3 interacts with both Lys^{48} and His^{81}. On the other hand, the modeled xylo-oligosaccharide chain shows that subsite −2 would be defined by the highly conserved Glu^{44}, Asn^{45}, and Trp^{291}, although the unconserved Tyr^{297} is protruding from the cleft and could possibly be involved in making interactions at subsites −2 or −3.

At the aglycone side of the binding cleft, the inhibitor phenyl located at subsite +1 is sandwiched in a hydrophobic pocket defined by Trp^{299} and Phe^{303} on one side, and Tyr^{179} on the other side. The presence of an additional aromatic residue, Phe^{303} in Xyn10B, seems to be a unique feature of intracellular xylanases, and it has previously been stated to be responsible for the increased catalytic efficiency of CmXyn10B against small

substrates (14). On the other hand, the main interaction previously described for bound xylose at subsite +2 is a stacking interaction to an aromatic residue, either a Phe/Trp in the above cited intracellular xylanases (14, 56) or a Tyr in other GH10 xylanases, a position that corresponds to His^{249} in Xyn10B. Other interactions at this subsite are highly variable among previously reported GH10 complexes. As can be observed in the figure, a part of the MPD2 molecule is located in the putative xylose placed at subsite +2, whereas the other part is pointing to a solvent-exposed pocket that is filled with a net of well ordered water molecules. This is a highly polar environment in which MPD2 does not make any direct interaction to Xyn10B even though Asp^{243}, Ser^{245}, Arg^{308}, and Asn^{310} contribute to keep it tightly bound to the active site by hydrogen bonding through water molecules. It is interesting to note that the change in His^{249} and Glu^{250} conformations observed in the Xy10B-R115 complex situates the His^{249} side chain at an almost interacting distance to the bound MPD2. This feature and the fact that the presence of a nonaromatic residue at this position is unique in Xyn10B suggest that His^{249} could possibly play an essential role in the enzymatic functionality of Xyn10B, as discussed below.

Docking Analysis of Xyn10B Active Site Suggests Possible Substrates—In view of the open cavity found in the structure of Xyn10B at subsite +2, and the high affinity shown by this enzyme *versus* the MPD2 molecule trapped in the crystal at this position, the possibility of binding decorated substrates was investigated by docking studies. It is well known that the xylan backbone may be substituted with acetyl or arabinose units at the O2 and O3 of xylosides, whereas 4-O-MeGlcA is only linked at O2. Therefore, models for a xylotriose chain with the internal ring decorated with either a 4-*O*-MeGlcA moiety modeled at O2 ($MeGlcA^2Xyl_3$) or an arabinose modeled at O3 (Ara^2Xyl_3) were built and automatically docked as flexible ligands into the aglycone portion of the active-site channel.

Using $MeGlcA^2Xyl_3$ as a ligand, the lowest total docking energy of −6.91 kcal/mol was obtained for a position in the highest ranked cluster (*orange* in Fig. 5*A*), which contained 27 out of 50 runs and had a mean docking energy of −5.68 kcal/mol. The second-ranked cluster (which accounts for 16 conformations with a mean binding energy of −3.93 kcal/mol) was situated similarly, but it was twisted in a way that the positions of the distal xylose (subsite +3) and that of the 4-*O*-MeGlcA rings were interchanged (*blue* in Fig. 5*A*). From the remaining seven conformations, only three had a negative docking energy (mean value of −0.25 kcal/mol), being very similar in position with the first-ranked cluster with a slightly different orientation of the 4-*O*-MeGlcA ring (not shown).

Interestingly, when the same calculation was performed with the Ara^2Xyl_3 ligand, a series of six very similar docking energy clusters were obtained. The first-ranked cluster is a low populated cluster (five conformations with a mean docking energy of −5.90 kcal/mol) containing the lowest energy state (−6.58 kcal/mol) that situates the arabinose decoration pointing to the solvent by means of a 180° flip of the ligand about the oligosaccharide chain axis (*orange* in Fig. 5*B*). The second- and third-ranked clusters are more populated (24 and 14 conformations, with mean energy of −5.75 and −5.85 kcal/mol, respectively)

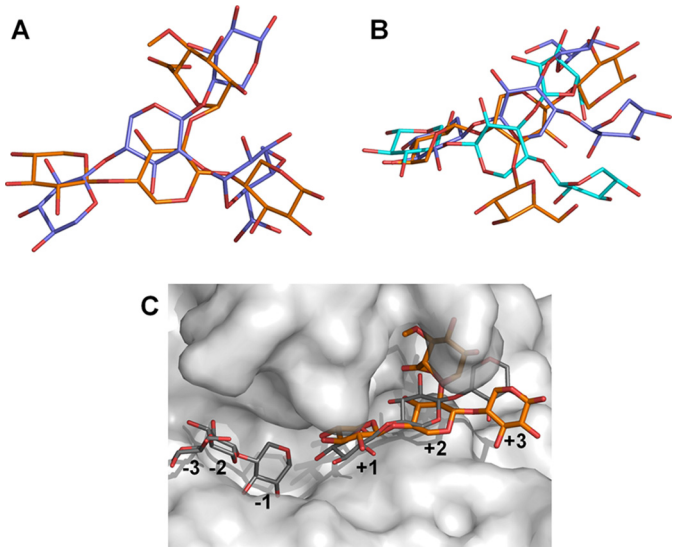

FIGURE 5. **Docking analysis of Xyn10B active site.** Decorated xylotriose ligands with 4-*O*-MeGlcA at O2 (*A*) and arabinose at O3 (*B*) were automatically docked into the crystal structure of Xyn10B and blocked at the aglycone portion of the active site with a fixed xylotriose chain. The lowest energy conformers of the first- and second-ranked cluster (*A*) and the first-, second-, and third-ranked cluster (*B*) are shown in *orange*, *blue*, and *cyan* and are explained under "Results." *C*, most energetically favorable conformer of *A* docked into the active site of Xyn10B superposes with the xylo-oligosaccharide chain inferred from structural superposition (*gray*) and situates the decoration in the wide cavity found at subsite +2.

and contain related ligand positions that involve a rotation of 180° about an axis perpendicular to the oligosaccharide chain that exchanges the reducing end by the nonreducing end (*blue* and *cyan* in Fig. 5*B*). It is noteworthy that the two last conformations place the arabinose decoration very similarly to that found with the $MeGlcA^2Xyl_3$ ligand.

In summary, docking analysis of xylotriose decorated at the O3 position with arabinose does not lead to any conclusion, as the conformations obtained are not chemically significant, *i.e.* none of them situates the xylose unit in a proper orientation within the +1 subsite for hydrolysis to proceed. On the contrary, xylotriose decorated with 4-*O*-MeGlcA at O2 docked into an energetically favorable conformation, a result consistent with the mapped subsites at the active site of Xyn10B. Fig. 5*C* displays the lowest energy conformer of the $MeGlcA^2Xyl_3$ ligand docked into the crystal structure, showing that it superposes with the inferred position of the oligosaccharide chain at the aglycone portion of the channel and situates the decoration in the wide cavity observed at subsite +2.

Activity of Xyn10B on glucuronic acid-decorated xylo-oligosaccharides was tested by TLC analysis of the hydrolysis products from branched xylo-oligomers. We analyzed the products released from aldohexaouronic acid (a xylopentaose with the central xylose O2 substituted with 4-*O*-MeGlcA, $MeGlcA^3Xyl_5$). It was cleaved to xylobiose and aldotetraouronic acid ($MeGlcA^3Xyl_3$), which corresponds to the substrate shortened in two xylose residues from its nonreducing end (Fig. 6). This product pattern suggests that Xyn10B has the requirement of binding to the −2 subsite for hydrolysis of short substrates, similarly to what has been reported for other GH10 xylanases (13, 60). This implies accommodation of the glucuronic acid ring of the tested substrate in +1, a subsite that

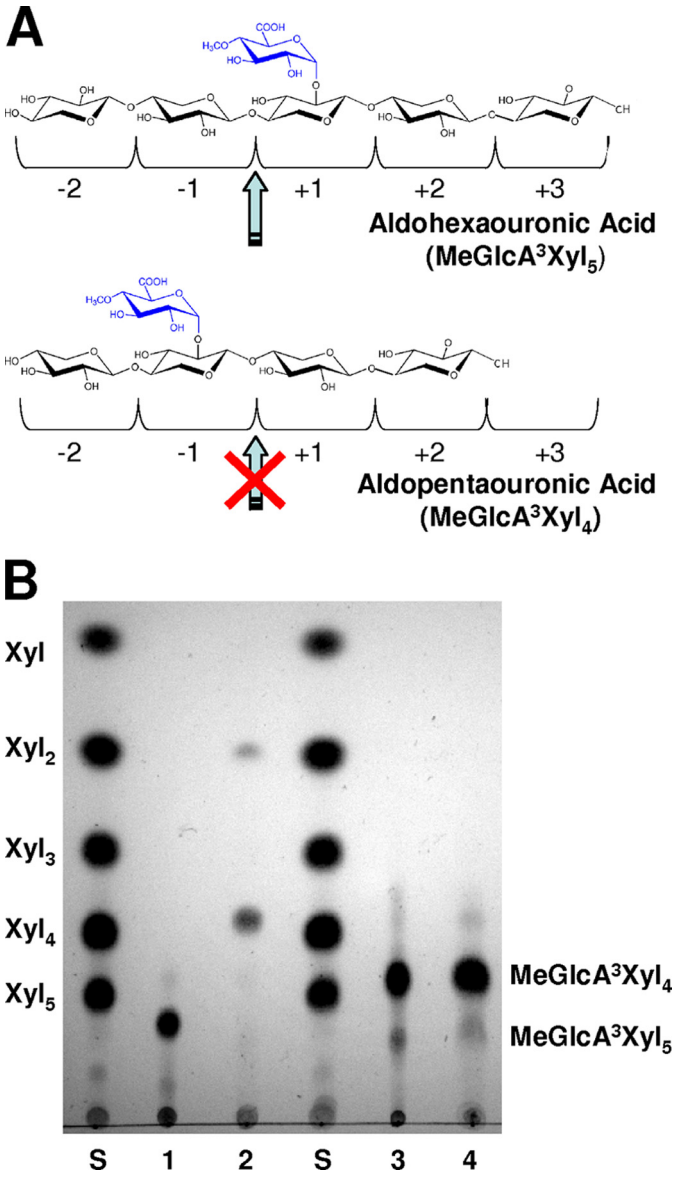

FIGURE 6. **Hydrolysis products from decorated xylo-oligomers.** *A,* schematic representation of oligomer cleavage by Xyn10B. *B,* TLC analysis of hydrolysis products from aldohexaouronic acid (MeGlcA^{3}Xyl$_5$) and aldopentaouronic acid (MeGlcA^{3}Xyl$_4$). Xyn10B was incubated with aldohexaouronic acid for 0 h (*lane 1*) or 2 h (*lane 2*) or with aldopentaouronic acid for 0 h (*lane 3*) or 2 h (*lane 4*). *Lanes S* contain standards of xylo-oligosaccharides from (xylose to xylopentaose).

admits decorations (14), but precludes its accommodation in the +2 cavity of *P. barcinonensis* Xyn10B. The affinity for this cavity would not be enough for productive binding of the substrate to subsites −1 to +4, which would leave an empty −2 subsite. The activity of the enzyme on a second decorated substrate, aldopentaouronic acid (a xylotetraose with the 4-*O*-MeGlcA substitution in the second xylose moiety from the nonreducing end, MeGlcA^{3}Xyl$_4$), was also evaluated (Fig. 6). This substrate was not cleaved by the enzyme, in accordance with the results shown above, suggesting the requirement of −2 subsite binding for hydrolysis. Binding to −2 subsite would imply accommodation of the glucuronic acid moiety of aldopentaouronic acid in the −1 subsite, where accommodation seems not to be allowed (14). Alternatively, accommodation of glucuronic acid decoration in the +2 cavity would place the bound oligomer out of the cleavage site. The design and availability of longer decorated xylo-oligosaccharides as aldoheptaouronic acid (MeGlcA^{3}Xyl$_6$), which could bind the −2 subsite and simultaneously accommodate in +2, would be required to analyze more deeply the mode of action of *P. barcinonensis* Xyn10B and the role of the +2 subsite cavity on substituent accommodation.

Directed Evolution of Xyn10B—The gene encoding Xyn10B was subjected to gene shuffling with the aim of obtaining xylanase mutants with increased thermal stability. In this way, *xyn10B* was amplified by PCR with *Taq* polymerase under conditions that promoted the misincorporation of nucleotides or, alternatively, under standard conditions. The amplified material was partially digested with DNase I and subjected to double-step PCR to reassemble full size *xyn10B* gene molecules. The reassembled molecules were ligated to the multicloning site of pGEM-T-easy and introduced in *E. coli* DH5α. About 2000 transformant clones were obtained and were subsequently screened for xylanase activity on solid media plates that were overlaid with *p*NPX. Those that produced enzymes that had retained xylanase activity after the mutagenic procedure were selected and evaluated for an increased thermal stability. The 85 active clones selected were inoculated in series of replica plates that, after growth, were flooded with chloroform, subjected to thermal shocks at 60, 70, or 80 °C for 15 min, and tested for residual xylanase activity by overlay assay with *p*NPX. Four of the clones produced a xylanase with increased thermostability compared with the wild type enzyme. They were selected, and their xylanase genes were sequenced. The following codon and amino acid substitutions were found: TCG→TTG (S15L), ATG→GTG (M93V), GAA→GAT (E137D), and GAT→AAT (D323N). The mutations that gave the amino acid changes E137D and D323N were found in a double mutant; mutation M93V was held by a single mutant, whereas mutation S15L was held by two identical single mutants. The selected mutants, except for the double mutant, derived from DNA shuffling of *xyn10B,* amplified under standard conditions.

Xyn10B Mutants Show Increased Catalytic Properties—Three of the isolated mutants contained, in addition to the described mutations, nucleotide changes that did not result in

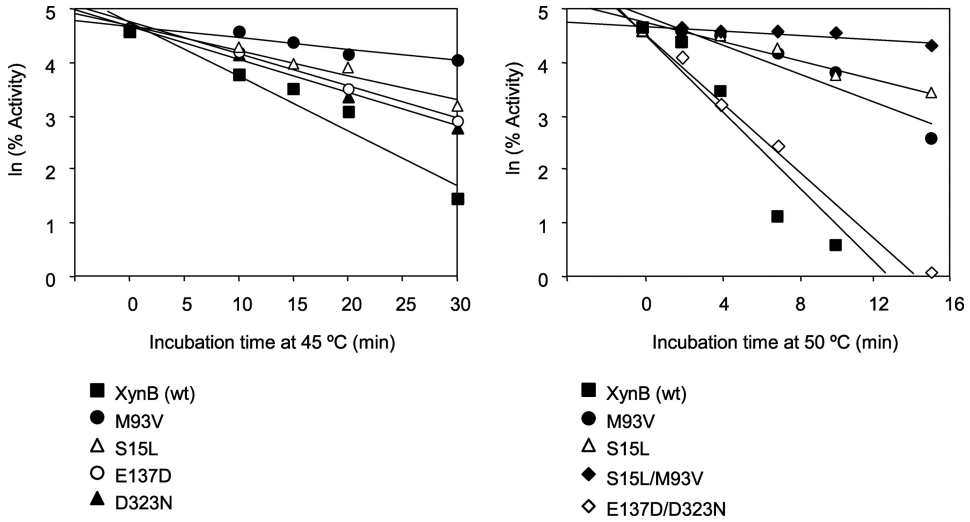

FIGURE 7. **Thermal inactivation of Xyn10B and mutant xylanases.** Purified xylanases were incubated at 45 or 50 °C in pH 7 buffer for increasing periods of time, and the residual activity was determined under standard conditions. The ln of percentage of residual activity is represented.

TABLE 2

Absolute and relative t_m values of wild type Xyn10B and mutant xylanases at 45 and 50 °C

t_m is the incubation time at a given temperature that causes a 50% irreversible thermal inactivation.

Enzyme	t_m, 45 °C	Relative t_m, 45 °C	t_m, 50 °C	Relative t_m, 50 °C
	min		*min*	
Xyn10B wild type	9.1	1	1.8	1
E137D	14.1	1.6		
D323N	11.2	1.2		
S15L	17.6	1.9	9.1	5.6
M93V	35.8	3.9	7.1	3.9
E137D/D323N			2.2	1.2
S15L/M93V			37.7	20.9

TABLE 3

Kinetic parameters of wild type Xyn10B and mutant xylanases

Enzyme	k_{cat}	K_m	k_{cat}/K_m
	min^{-1}	M	$min^{-1}\,M^{-1}$
Xyn10B wild type	7.80×10^3	2.834×10^{-3}	3.27×10^6
S15L	6.93×10^4	1.820×10^{-3}	3.81×10^7
M93V	7.06×10^4	1.712×10^{-3}	4.13×10^7
S15L/M93V	5.48×10^4	1.497×10^{-3}	3.66×10^7
E137D/D323N	9.64×10^4	2.495×10^{-3}	3.86×10^7

changes in the amino acid sequence of the xylanase. To remove these noncoding nucleotide changes, the identified mutations were individually introduced in wild type *xyn10B* by site-directed mutagenesis. In this way, four mutant xylanases were constructed, one for each of the mutations identified. The four mutant enzymes, S15L, M93V, E137D, and D323N, were purified to homogeneity, and their thermal resistance was evaluated. Fig. 7 shows the irreversible thermal inactivation of the mutant xylanases at 45 and 50 °C. The four mutant enzymes showed an increased stability when compared with the wild type enzyme. The highest stabilities were shown by S15L and M93V xylanases that displayed half-lives at 50 °C five and four times longer than that of wild type purified xylanase (Table 2).

Mutations that increase thermal stability of enzymes often show additive or cooperative effects when they are combined in the same sequence. To test if the combination of the mutations identified produced an enhanced increase in thermal resistance of Xyn10B, we constructed two double mutants by site-directed mutagenesis. The S15L/M93V mutant combined the single mutations that caused higher stabilization of the enzyme, whereas the E137D/D323N mutant contained the two mutations that had initially been isolated from the same original clone. Double mutant xylanases were purified to homogeneity, and thermal inactivation at 50 °C was evaluated. S15L/M93V xylanase exhibited a considerably higher stability than wild type Xyn10B (around 20 times longer half-life), showing the cooperative effect of the two single mutations it contained in the stabilization of the enzyme. The second double mutant constructed E137D/D323N did not show any substantial increase in thermal stability at 50 °C when compared with the wild type xylanase.

The kinetic parameters of wild type and mutant xylanases on *p*NPX were evaluated. Wild type enzyme showed a K_m of 2.834 mM and a k_{cat} value of 7.80×10^3 min^{-1} (Table 3). The mutant xylanases showed a slightly increased affinity that in the case of S15L/M93V was 1.497 mM. However, the thermostable mutants displayed a notably enhanced k_{cat} value (5.48×10^4 min^{-1} in the case of S15L/M93V xylanase) when compared with the wild type enzyme. Thus, all mutants showed an increased catalytic efficiency, expressed as the k_{cat}/K_m ratio, that was about 10-fold higher than that of the wild type enzyme, which showed a catalytic efficiency of 3.27×10^6 min^{-1} M^{-1}. Comparison of the kinetic parameters of wild type Xyn10B with other GH10 xylanases shows a higher activity on *p*NPX than other reported xylanases, such as CmXyn10B that shows a k_{cat}/K_m of 2.1×10^2 min^{-1} M^{-1} on the same substrate (14). The results found are in agreement with previous reports showing that Xyn10B from *P. barcinonensis* is highly active on aryl-xylosides, and it shows higher specific activity on *p*NPX than on xylans, which makes it unique among known xylanases (26, 38). The unusual high activity on aryl-xylosides such as *p*NPX could reflect a strong binding of *p*-nitrophenyl moiety of *p*NPX to the +1 subsite, where, as mentioned previously, the additional aromatic residue (Phe^{303} in Xyn10B) of intracellular xylanases can be responsible for an increased catalytic activity on small substrates (14). However, the similarity of the +1 subsite between intracellular xylanases does not correlate with the differences in activity on *p*NPX found among these enzymes.

DISCUSSION

Xylan degradation requires the coordinate action of several enzymes, among which the recently described intracellular xylanases may play an important role for the effective utiliza-

tion of xylan in natural environments. Although most of xylanases are enzymes secreted to the extracellular medium to get contact with and to depolymerize xylan, a big sized substrate, several intracellular xylanases have been described in both Gram-positive and Gram-negative microorganisms. The significance of intracellular xylanases on xylan degradation is not clear, although their natural substrates should be xylo-oligomers produced by the action of extracellular xylanases, once they have been transported inside the cells by membrane transporters, as those described for *G. stearothermophilus* (61) and *Streptomyces thermoviolaceus* (62). It has been suggested that intracellular xylanases would be protected against external factors such as proteases that may lead to their inactivation (25), or alternatively, this would be a way to sequester the polysaccharide hydrolysis products from competing microorganisms (63). A main difference among intracellular xylanases crystallized to date is their location inside the cells. Two different subcellular locations have been described. Whereas *C. mixtus* Xyn10B (CmXyn10B) shows a twin arginine signal peptide and is located in the periplasmic space (25), signal peptide-less *P. barcinonensis* Xyn10B is located in the cytoplasm of cells (26). Cytoplasm or periplasm could be two options of the same strategy to internalize enzymes. The different location could be correlated to the different cell wall structure, Gram-positive or Gram-negative, of the producing microorganism. In accordance with the proposed physiological function of intracellular xylanases, *P. barcinonensis* Xyn10B shows high activity on xylo-oligosaccharides (26, 38). Similar high activity on short substrates has been reported for CmXyn10B (14), although no data have been reported about activity on xylo-oligosaccharides of *G. stearothermophilus* intracellular xylanase (GsXynB).

P. barcinonensis Xyn10B shows high homology (more than 50% of identity) to the group of signal peptide-less xylanases mentioned above, although homology to periplasmic CmXyn10B is much lower. Signal peptide-less xylanases show the distinctive conserved amino acid sequence regions a and b in helix α6 and loop L7, probably as a result of their phylogenetic proximity, as they cluster in a separate group of xylanases (26). However, the few existing reports on the biochemical characterization of signal peptide-less xylanases precludes further conclusions about the catalytic properties shared by these enzymes.

One of the most notable features of Xyn10B structure is the wide cavity observed at subsite +2. This pocket is a highly polar environment modulated by Arg^{248}, His^{249}, and Glu^{250}, located in close sequence proximity to region b (residues 253–263). In contrast to the His^{249} residue found at subsite +2 of *P. barcinonensis* Xyn10B, aromatic residues are found in other xylanases such as CmXyn10B and GsXynB, which bear residues Trp^{272} and Phe^{249} at this subsite, respectively. As a result they have a narrower cleft at the aglycon-binding site, which in the case of GsXynB has been proposed to be the one of the shortest among family 10 xylanases (56). From the structure of *P. barcinonensis* Xyn10B subsite +2, and considering the docking analysis results, we suggest that its active-site cavity may accommodate glucuronic acid-substituted xylose residues contained in branched oligosaccharides. These results differ from those reported in CmXyn10B, where decorations cannot be accommodated at subsite +2 (14), or in *S. olivaceoviridis* SoXyn10A, where only arabinose can be tolerated at the O2 position of the xylose located in this subsite (15). Sequence analysis of signal peptide-less xylanases revealed that all these enzymes have aromatic residues at the position corresponding to His^{249} from *P. barcinonensis* Xyn10B, with the exception of *A. caviae* XynX, which also has a His^{249} residue at this position (32). The two latter enzymes are highly homologous (85% identity) and have in common that they hydrolyze xylan releasing as main products xylobiose and a substituted tetrasaccharide previously considered as xylotetraose (32, 38). This probably reflects a structural similarity of the enzymes that, besides the distinctive region b, show high amino acid sequence homology in the rest of L7 loop. A deeper study of the two enzymes will be necessary to compare them and reveal their specific function in plant xylan degradation.

Four mutations that increase thermal stability of Xyn10B have been identified, two of which, S15L and M93V, gave rise to a notable stabilization of the enzyme against temperature. Residue Ser^{15} is located in an external loop near the N terminus of the enzyme, before β1. Its substitution by a Leu made the enzyme more resistant to thermal inactivation, and indeed S15L was the mutation that caused a higher stabilization of Xyn10B. The crystal structure of the enzyme shows that Ser^{15} is located in a shallow indentation of the enzyme, forming hydrogen bonds to Arg^{282} side chain and the carboxylic C-terminal group of Asp^{332}, at the enzyme surface (Fig. 8*A*). Its replacement by Leu in mutant xylanase S15L (Fig. 8*B*) precludes the formation of these hydrogen bonds, but it should probably not disrupt the existing link between the polypeptide C terminus and Arg^{282} at the end of helix α7. This link might be essential for keeping the stability of the C terminus, which, as deduced from the electron density map, is well ordered. Moreover, computer modeling of mutant xylanase S15L displayed in the figure shows that putative Leu^{15} would be at an interacting distance not only with the underlying aromatic residues Tyr^{12} and Phe^{16} but also with the aliphatic moiety of Arg^{279} and Arg^{282}. Hydrophobic interaction with these residues can improve the packing efficiency giving a more compact enzyme structure. Additionally, the branched side chain of Leu^{15} can better fill the shallow depression on the protein surface than wild type Ser, yielding a more efficient structure (Fig. 8, *C* and *D*) at this region, which includes the beginning and the end of the polypeptide chain and also the α8 helix of the barrel. This would result in an increased resistance to denaturation and a more stable xylanase. A similar stabilization effect caused by the replacement of a surface polar residue by a hydrophobic amino acid has been reported for the mesophilic cold shock protein from *Bacillus subtilis,* which can be converted into a highly thermostable form by changing Glu surface residues to Leu or to Val (22, 24). Although it is generally assumed that hydrophobic residues are not favorable at solvent-exposed sites, it has been shown that introduction of hydrophobic residues at protein surface can result in a stabilization effect (23). In the work reported by Machius *et al.* (23), the replacement by Val of wild type Ala or His residues that lay in small surface grooves between secondary structure elements increased hydrophobic packing within these

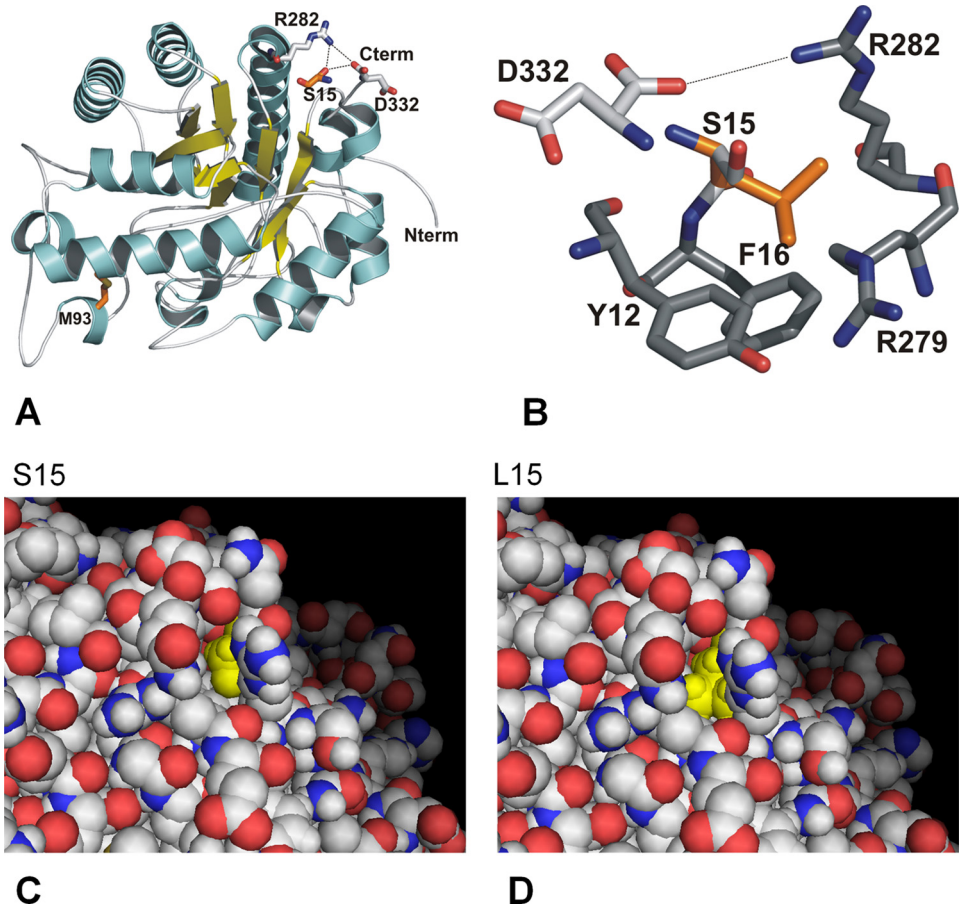

FIGURE 8. **Structural basis for the thermoresistance in the mutants.** *A,* location of the residues that increase the thermal stability of Xyn10B; Ser^{15} is located before β1, in a short external loop making polar interactions with Arg^{282}, at the end of helix α7, and the carboxylic C terminus (*Cterm*) of Asp^{332}; Met^{93} is located in loop L3 at the protein surface. *B,* close view of the atomic interactions of the modeled S15L substitution showing hydrophobic contacts of the putative Leu (*orange*). *C* and *D,* molecular representation of Xyn10B (*left*) and modeled S15L mutant (*right*) showing the change in the surface pocket suggested by the amino acid substitution (in *yellow*) and that the putative Leu side chain may shield the hydrophobic cluster from the solvent. *Nterm,* N terminus.

indentations. This led to the reinforcement of hydrophobic contact between the secondary structure elements and to the shielding from solvent of buried hydrophobic clusters. Creation of a hydrophobic shield protecting secondary structures against water molecules has also been proposed to explain the stabilizing effects of surface-located mutations in a thermophilic protease (64).

As shown in Fig. 8*A*, Met^{93} is located in loop L3 between β3 and α3, at the surface of Xyn10B. The stabilization of the enzyme provided by M93V mutation is probably due to the protection against oxidation at high temperatures. Given the susceptibility of methionine to oxidation (65), elimination of this labile residue from the surface of the enzyme and its replacement by Val would protect Xyn10B against oxidative inactivation and would render the enzyme more resistant to irreversible thermal denaturation. A similar mutation has been reported in β-glucosidase B from *Paenibacillus polymyxa* (66), where the replacement of Met by more chemically stable residues such as Val or Ile gave rise to an increase in thermal stability of the enzyme. The crystal structure of Xyn10B shows that wild type Met is located in a cavity at the surface of the enzyme. In addition to the resistance to oxidation proposed for M93V mutation, Met replacement by Val could contribute to an improved hydrophobic packing with neighbor residues Trp^{92} and Phe^{94}, yielding a more compact structure, similarly to the effects proposed for mutation S15L.

Analysis of the kinetic parameters showed that mutant enzymes do not exhibit substantial differences in affinity compared with wild type Xyn10B, although they show about a 10-fold enhancement in k_{cat}/K_m values. This increased catalytic efficiency could be due to a local stabilization of the catalytic site as a consequence of the higher thermal stability of the enzyme. At this respect, there are several examples showing mutations that increase thermal resistance without compromising the catalytic efficiency of enzymes, and even hyperstable variants of certain enzymes have been obtained that retain their activity (67). In other instances, mutant enzymes with simultaneous enhancement of stability and activity have been reported (66, 68). On the other hand, analysis by circular dichroism of wild type and double mutant S15L/M93V xylanases shows no significant differences in secondary structure (data not shown), although small differences detected at 228–240 nm can be correlated to subtle structural differences in the aromatic clusters, in agreement with the predicted environment of the S15L mutant mentioned above.

Random mutagenesis and directed evolution are widely used to improve the properties of enzymes and to show that there are many strategies that lead to higher stability of the enzymes, most of them not easy to predict or rationalize (20). All the mutations studied in our work are located in loops at superficial positions in the three-dimensional structure of the enzyme. The stabilizing effect found supports the increased awareness of the importance of protein surface for stability.

To conclude, this study shows that forced protein evolution can be used to produce enzymes that display improved thermostability and that this can be achieved by introduction of very few changes in the sequence, as reported previously (21, 20). More structural knowledge is still needed to develop general principles for stabilization strategies of enzymes, a task that will be accomplished when the structural basis for the stability is fully understood. Detailed structural information also helps in revealing unexpected

new features of enzymes, as is the case of the unusual cavity found at the +2 active subsite of Xyn10B, which possibly points to an unpredicted activity of this enzyme. The final goal of this extensive structural approach will be the generation of improved and more resistant biocatalysts with functionalities most suitable for industrial purposes.

Acknowledgment—We thank Professor Peter Biely for the gift of aldohexaouronic and aldotretraouronic acids.

REFERENCES

1. Kulkarni, N., Shendye, A., and Rao, M. (1999) *FEMS Microbiol. Rev.* **23,** 411–456
2. Collins, T., Gerday, C., and Feller, G. (2005) *FEMS Microbiol. Rev.* **29,** 3–23
3. Henrissat, B., and Davies, G. J. (1997) *Curr. Opin. Struct. Biol.* **7,** 637–644
4. Larson, S. B., Day, J., Barba de la Rosa, A. P., Keen, N. T., and McPherson, A. (2003) *Biochemistry* **42,** 8411–8422
5. Van Petegem, F., Collins, T., Meuwis, M. A., Gerday, C., Feller, G., and Van Beeumen, J. (2003) *J. Biol. Chem.* **278,** 7531–7539
6. Harris, G. W., Jenkins, J. A., Connerton, I., Cummings, N., Lo Leggio, L., Scott, M., Hazlewood, G. P., Laurie, J. I., Gilbert, H. J., and Pickersgill, R. W. (1994) *Structure* **2,** 1107–1116
7. Lo Leggio, L., Kalogiannis, S., Bhat, M. K., and Pickersgill, R. W. (1999) *Proteins Struct. Funct. Genet.* **36,** 295–306
8. Wakarchuk, W. W., Campbell, R. L., Sung, W. L., Davoodi, J., and Yaguchi, M. (1994) *Protein Sci.* **3,** 467–475
9. Sidhu, G., Withers, S. G., Nguyen, N. T., McIntosh, L. P., Ziser, L., and Brayer, G. D. (1999) *Biochemistry* **38,** 5346–5354
10. Rye, C. S., and Withers, S. G. (2000) *Curr. Opin. Chem. Biol.* **4,** 573–580
11. Biely, P., Vrsanská, M., Tenkanen, M., and Kluepfel, D. (1997) *J. Biotechnol.* **57,** 151–166
12. Vrsanská, M., Kolenová, K., Puchart, V., and Biely, P. (2007) *FEBS J.* **274,** 1666–1677
13. Kolenová, K., Vrsanská, M., and Biely, P. (2006) *J. Biotechnol.* **121,** 338–345
14. Pell, G., Taylor, E. J., Gloster, T. M., Turkenburg, J. P., Fontes, C. M., Ferreira, L. M., Nagy, T., Clark, S. J., Davies, G. J., and Gilbert, H. J. (2004) *J. Biol. Chem.* **279,** 9597–9605
15. Fujimoto, Z., Kaneko, S., Kuno, A., Kobayashi, H., Kusakabe, I., and Mizuno, H. (2004) *J. Biol. Chem.* **279,** 9606–9614
16. Vardakou, M., Flint, J., Christakopoulos, P., Lewis, R. J., Gilbert, H. J., and Murray, J. W. (2005) *J. Mol. Biol.* **352,** 1060–1067
17. Viikari, L., Kantelinen, A., Sundquist, J., and Linko, M. (1994) *FEMS Microbiol. Rev.* **13,** 335–350
18. Polizeli, M. L., Rizzatti, A. C., Monti, R., Terenzi, H. F., Jorge, J. A., and Amorim, D. S. (2005) *Appl. Microbiol. Biotechnol.* **67,** 577–591
19. Tabka, M. G., Herpoël-Gimbert, I., Monod, F., Asther, M., and Sigoillot, J. C. (2006) *Enzyme Microb. Technol.* **39,** 897–902
20. Eijsink, V. G., Bjørk, A., Gåseidnes, S., Sirevåg, R., Synstad, B., van den Burg, B., and Vriend, G. (2004) *J. Biotechnol.* **113,** 105–120
21. Sandgren, M., Gualfetti, P. J., Shaw, A., Gross, L. S., Saldajeno, M., Day, A. G., Jones, T. A., and Mitchinson, C. (2003) *Protein. Sci.* **12,** 848–860
22. Martin, A., Kather, I., and Schmid, F. X. (2002) *J. Mol. Biol.* **318,** 1341–1349
23. Machius, M., Declerck, N., Huber, R., and Wiegand, G. (2003) *J. Biol. Chem.* **278,** 11546–11553
24. Perl, D., Mueller, U., Heinemann, U., and Schmid, F. X. (2000) *Nat. Struct. Biol.* **7,** 380–383
25. Fontes, C. M., Gilbert, H. J., Hazlewood, G. P., Clarke, J. H., Prates, J. A., McKie, V. A., Nagy, T., Fernandes, T. H., and Ferreira, L. M. (2000) *Microbiology* **146,** 1959–1967
26. Gallardo, O., Diaz, P., and Pastor, F. I. (2003) *Appl. Microbiol. Biotechnol.* **61,** 226–233
27. Usui, K., Suzuki, T., Akisaka, T., and Kawai, K. (2003) *J. Biosci. Bioeng.* **95,** 488–495
28. Sánchez, M. M., Fritze, D., Blanco, A., Spröer, C., Tindall, B. J., Schumann, P., Kroppenstedt, R. M., Diaz, P., and Pastor, F. I. (2005) *Int. J. Syst. Evol. Microbiol.* **55,** 935–939
29. Blanco, A., Vidal, T., Colom, J. F., and Pastor, F. I. (1995) *Appl. Environ. Microbiol.* **61,** 4468–4470
30. Blanco, A., Díaz, P., Zueco, J., Parascandola, P., and Javier Pastor, F. I. (1999) *Microbiology* **145,** 2163–2170
31. Torres, A. L., Roncero, M. B., Colom, J. F., Pastor, F. I., Blanco, A., and Vidal, T. (2000) *Bioresource Technol.* **74,** 135–140
32. Usui, K., Ibata, K., Suzuki, T., and Kawai, K. (1999) *Biosci. Biotechnol. Biochem.* **63,** 1346–1352
33. Shulami, S., Gat, O., Sonenshein, A. L., and Shoham, Y. (1999) *J. Bacteriol.* **181,** 3695–3704
34. Tabernero, C., Sánchez-Torres, J., Pérez, P., and Santamaría R. I. (1995) *Appl. Environ. Microbiol.* **61,** 2420–2424
35. Baba, T., Shinke, R., and Nanmori, T. (1994) *Appl. Environ. Microbiol.* **60,** 2252–2258
36. Connerton, I., Cummings, N., Harris, G. W., Debeire, P., and Breton, C. (1999) *Biochim. Biophys. Acta* **1433,** 110–121
37. Lüthi, E., Love, D. R., McAnulty, J., Wallace, C., Caughey, P. A., Saul, D., and Bergquist, P. L. (1990) *Appl. Environ. Microbiol.* **56,** 1017–1024
38. Blanco, A., Díaz, P., Martínez, J., López, O., Soler, C., and Pastor, F. I. (1996) *FEMS Microbiol. Lett.* **137,** 285–290
39. Fromant, M., Blanquet, S., and Plateau, P. (1995) *Anal. Biochem.* **224,** 347–353
40. Liao, X. B., and Wise, J. A. (1990) *Gene* **88,** 107–111
41. Gonzalez-Blasco, G., Sanz-Aparicio, J., Gonzalez, B., Hermoso, J. A., and Polaina, J. (2000) *J. Biol. Chem.* **275,** 13708–13712
42. Stemmer, W. P. (1994) *Proc. Natl. Acad. Sci. U.S.A.* **91,** 10747–10751
43. Lopez-Camacho, C., and Polaina, J. (1993) *Mutat. Res.* **301,** 73–77
44. Mikaelian, I., and Sergeant, A. (1992) *Nucleic Acids Res.* **20,** 376
45. Lopez-Camacho, C., Salgado, J., Lequerica, J. L., Madarro, A., Ballestar, E., Franco, L., and Polaina, J. (1996) *Biochem. J.* **314,** 833–838
46. Otwinowski, Z., and Minor, W. (1997) *Methods Enzymol.* **276,** 307–326
47. Vagin, A., and Teplyakov, A. (1997) *J. Appl. Crystallogr.* **30,** 1022–1025
48. Brünger, A. T., Adams, P. D., Clore, G. M., DeLano, W. L., Gros, P., Grosse-Kunstleve, R. W., Jiang, J. S., Kuszewski, J., Nilges, M., Pannu, N. S., Read, R. J., Rice, L. M., Simonson, T., and Warren, G. L. (1998) *Acta Crystallogr. D Biol. Crystallogr.* **54,** 905–921
49. Jones, T. A., Zou, J. Y., Cowan, S. W., and Kjeldgaard, M. (1991) *Acta Crystallogr. A* **47,** 110–119
50. Laskowsky, R. A., MacArthur, M. W., Moss, D. S., and Thornton, J. M. (1993) *J. Appl. Crystallogr.* **26,** 283–291
51. Davis, I. W., Leaver-Fay, A., Chen, V. B., Block, J. N., Kapral, G. J., Wang, X., Murray, L. W., Arendall, W. B., 3rd, Snoeyink, J., Richardson, J. S., and Richardson, D. C. (2007) *Nucleic Acids Research* **35,** W375–W383
52. DeLano, W. L. (2002) *The PyMOL Molecular Graphics System,* DeLano Scientific LLC, San Carlos, CA
53. Sanner, M. F. (1999) *J. Mol. Graph. Model* **17,** 57–61
54. Morris, G. M., Goodsell, D. S., Halliday, R. S., Huey, R., Hart, W. E., Belew, R. K., and Oldson, A. J. (1998) *J. Comput. Chem.* **19,** 1639–1662
55. Fukumura, M., Sakka, K., Shimada, K., and Ohmiya, K. (1995) *Biosci. Biotechnol. Biochem.* **59,** 40–46
56. Solomon, V., Teplitsky, A., Shulami, S., Zolotnitsky, G., Shoham, Y., and Shoham, G. (2007) *Acta Crystallogr. D Biol. Crystallogr.* **63,** 845–859
57. Biely, P., Krátký, Z., and Vrsanská, M. (1981) *Eur. J. Biochem.* **119,** 559–564
58. Davies, G. J., Wilson, K. S., and Henrissat, B. (1997) *Biochem. J.* **321,** 557–559
59. Łysek, R., Schütz, C., and Vogel, P. (2005) *Bioorg. Med. Chem. Lett.* **15,** 3071–3075
60. Charnock, S. J., Spurway, T. D., Xie, H., Beylot, M. H., Virden, R., Warren, R. A., Hazlewood, G. P., and Gilbert, H. J. (1998) *J. Biol. Chem.* **273,** 32187–32199
61. Shulami, S., Zaide, G., Zolotnitsky, G., Langut, Y., Feld, G., Sonenshein, A. L., and Shoham, Y. (2007) *Appl. Environ. Microbiol.* **73,** 874–884
62. Tsujibo, H., Kosaka, M., Ikenishi, S., Sato, T., Miyamoto, K., and Inamori, Y. (2004) *J. Bacteriol.* **186,** 1029–1037

63. Miyazaki, K., Martin, J. C., Marinsek-Logar, R., and Flint, H. J. (1997) *Anaerobe* **3,** 373–381
64. Frigerio, F., Margarit, I., Nogarotto, R., de Filippis, V., and Grandi, G. (1996) *Protein Eng.* **9,** 439–445
65. Estell, D. A., Graycar, T. P., and Wells, J. A. (1985) *J. Biol. Chem.* **260,** 6518–6521
66. Arrizubieta, M. J., and Polaina, J. (2000) *J. Biol. Chem.* **275,** 28843–28848
67. Van den Burg, B., Vriend, G., Veltman, O. R., Venema, G., and Eijsink, V. G. (1998) *Proc. Natl. Acad. Sci. U.S.A.* **95,** 2056–2060
68. Yasukawa, K., and Inouye, K. (2007) *Biochim. Biophys. Acta* **1774,** 1281–1288